Insights into agricultural influences and weathering processes from major ion patters

Robert van Geldern[1,]*, Peter Schulte[1,2], Michael Mader[1], Alfons Baier[1], Johannes A.C. Barth[1], Tobias R. Juhlke[1], Kern Lee[1]

[1] *Friedrich-Alexander-University Erlangen-Nuremberg (FAU), Department of Geography and Geosciences, GeoZentrum Nordbayern, Schlossgarten 5, 91054 Erlangen, Germany*

[2] *Gehrenhagweg 6, CH-5420 Ehrendingen, Switzerland*

*Corresponding author.

robert.van.geldern@fau.de. phone +49 9131 8522514. fax +49 9131 29294.

1   **ABSTRACT**

2   Karst areas and their catchments pose a great challenge for protection because fast conduit

3   flow results in low natural attenuation of anthropogenic contaminants. Studies of the

4   hydrochemistry of karst sources and river solutes are an important tool for securing and

5   managing water resources. A study of the geochemical downriver evolution of the Wiesent

6   River and its tributaries, located in a typical karst terrain, revealed unexpected downstream

7   decreases of nitrate with maximum mean values of 30 mg L^{-1} at the source to minimum

8   values of 18 mg L^{-1} near the river mouth. This trend persisted over the length of the river

9   even though increased agricultural activities are evident in the downstream section of the

10 catchment. This pattern is caused by fertilizer inputs via diffusive and fast conduits flow from

11 karst lithology in the upstream area that may have reached the river's source even from

12 beyond the hydrological catchment boundaries. Further downstream, these influences became

13 diluted by tributary inputs that drain subcatchments dominated by claystone and sandstone

14 lithologies that increased potassium and sulfate concentrations. Our findings indicate that

15 bedrock geology remains the dominant control on the major ion chemistry of the Wiesent

16 River, and that agricultural influences are strongest near the headwaters despite increased

17 land-use further downstream, due to long-term storage and accumulation in karst aquifers.

18 This feature may not be unique to the Wiesent River system, as carbonates cover significant

19 portions of the Earth's surface and subsequent work in other river systems could establish

20 whether such patterns are ubiquitous worldwide.

21

24 **INTRODUCTION**

25   Clean freshwater is essential to life. The most accessible form of freshwater is river

26 and lake water, but it constitutes only a small fraction of less than 0.3% of the Earth's

27 available total freshwater (Gleick, 1996). Groundwater is more abundant (30%), but a less

28 accessible form of freshwater that is primarily replenished by recharge from precipitation. All

29 three surficial compartments of the hydrologic cycle – precipitation, rivers and lakes, and

30 groundwater – are hydrologically interconnected. Studying the hydrochemistry of river

31 solutes and suspended matter is therefore of importance for securing and managing this

32 essential resource.

33   The factors controlling the chemical evolution of numerous of the world's largest river

34 systems has been examined in several studies worldwide (Négrel *et al.*, 1993; Yang *et al.*,

35 1996; Gaillardet *et al.*, 1997; Aucour *et al.*, 1999; Galy and France-Lanord, 1999; Zhang *et*

36 *al.*, 1999; Kendall *et al.*, 2001; Biggs *et al.*, 2002; Hélie *et al.*, 2002; Richey *et al.*, 2002;

37 Szramek *et al.*, 2007; Chetelat *et al.*, 2008; Raymond *et al.*, 2008; Cartwright, 2010; Rosa *et*

38 *al.*, 2012; Voss *et al.*, 2014). From their headwater catchments to their eventual confluence to

39 the oceans, rivers act as a major global transportation network for water and solutes. Riverine

40 continental fluxes of major elements, nutrients, and carbon phases were subsequently

41 evaluated on a global scale (Gibbs, 1970; Meybeck, 1982; Meybeck, 1987; Gaillardet *et al.*,

42 1999; Viers *et al.*, 2009; Seitzinger *et al.*, 2010; Aufdenkampe *et al.*, 2011; Milliman and

43 Farnsworth, 2011; Raymond *et al.*, 2013; Marx *et al.*, 2017a). Following these studies,

44 numerous studies on smaller catchments and river systems were also carried out (e.g., Probst

45 *et al.*, 1992; Flintrop *et al.*, 1996; Grosbois *et al.*, 2000; Barth *et al.*, 2003; Kanduč *et al.*,

46 2007; Soulsby *et al.*, 2007; Doctor *et al.*, 2008; Stögbauer *et al.*, 2008; Brunet *et al.*, 2011;

47 Kanduč *et al.*, 2012; Kanduč *et al.*, 2013; Zavadlav *et al.*, 2013; Daesslé *et al.*, 2016; Daesslé

48   *et al.*, 2017; Lee *et al.*, 2017; Marx *et al.*, 2017b), and most of these showed increasing

49   conductivities and fluxes with closer proximity to confluences with larger river systems. This

50   trend corresponds to increasing element loads further downstream and is usually related to

51   increasing anthropogenic activities, including traffic infrastructure, settlements and

52   agricultural practices in the downstream sections of catchments.

53   Karst areas and their rivers exhibit a great challenge to the protection of freshwater

54   resources because fast conduit flow results in low natural attenuation of anthropogenic

55   derived contaminants (Bakalowicz, 2005). These conduit systems make karst aquifers highly

56   vulnerable to anthropogenic pollution, for example by nitrate (NO_3^-), because of the virtual

57   absence of filter effects that are common in pore aquifers. Moreover, it is known that

58   fertilizers can lower pH values and thus cause additional weathering that in turn should be

59   particularly pronounced in karst that is susceptible to acidity changes (Semhi *et al.*, 2000;

60   Perrin *et al.*, 2008; Gandois *et al.*, 2011).

61   Here we present a small river system of 72.4 km length, the Wiesent River (Figure 1).

62   Being dominated by karst lithology, it was first studied as an ideal natural laboratory for

63   investigations of the aqueous carbon cycle in karst areas and its response to excessive carbon

64   loss to the atmosphere, particularly in its source region (van Geldern *et al.*, 2015). The

65   catchment is situated in a dolomite and calcite-dominated terrain that trends towards shale and

66   sandstone terrains in the lower reaches of the river (Figure 1). This allows for interpretations

67   of spatial heterogeneity in river water chemistry, while sampling over a period of almost one

68   year enabled temporal interpretations of seasonal variations in riverine solutes, carbon

69   transport, CO_2 evasion and associated changes in the carbon isotope distribution of dissolved

70   inorganic carbon (DIC).

71   The objectives of this study were to assess the spatial and temporal downriver

72   evolution of major ion chemistry in a typical karst river with the initial hypothesis of a

73   continuous increase of solutes along the flow path of the river. In particular, we investigated if

74   such a trend could be observed in our data set. With this in mind, we evaluate relative

75   influences of natural versus anthropogenic impacts, together with the role of groundwater

76   contributions along the river course. This will advance the understanding of source-related

77   inputs while providing information on the dilution of anthropogenic and weathering inputs in

78   space and time. Regarding the high vulnerability of karst terrains by agricultural land use and

79   anthropogenic pollution, this is of particular interest with regard to the ecological functioning

80   of rivers with significant proportions of limestone in their catchment lithology.

81   **STUDY AREA**

82   The Wiesent River catchment with a total area of 1,040 km^2 is located in southern

83   Germany (Figure 1). The source of the Wiesent River is located in the northwest of the

84   catchment area, at the hamlet of Steinfeld (our sampling site no. 1) at 445 meters above sea

85   level (m.a.s.l.) (Figure 1). From this point, the river flows in a southeast to south direction.

86   Near the town of Goessweinstein, the general flow direction changes westward until the river

87   finally reaches the Regnitz River at 250 m.a.s.l. A map showing the digital elevation model

88   (DEM) (Figure S1) is available from the Supplementary Material to this article.

89   The total length of the Wiesent River is 72.4 km and the most important tributaries are

90   the rivers Kainach, Truppach, Puettlach, Aufsess, Leinleiter, and Trubach (Figure 1). Two

91   discharge gauges are located along the main river at the villages of Hollfeld and Muggendorf.

92   They show averaged long-term discharge values of 1.04 m^3 s^{-1} and 7.11 m^3 s^{-1}, respectively

93   (LfU, 2014).

94   The study area is located in a karst region with lithologies of calcites and dolomites

95   that are occasionally interbedded with marly layers. These sediments form the Franconian

96   Jura uplands, which belong to the Franconian Alb that is part of the South German

97   Scarplands. Overall, late Jurassic carbonates cover the majority (~67%) of the catchment area

98   (Figure 1). These comprise a limestone sequence of up to 200 m thickness that is in part

99   dolomitized, and forms a typical karst landscape of the area with incised rivers and other dry

100 valleys, dolines and caverns (Figure 2). This carbonate sequence is overlain by relict patches

101 of Late Cretaceous sandstone with interbedded marl and shale layers.

102   All sedimentary layers dip at a shallow angle in an eastward direction. As a

103 consequence, lower Jurassic and Late Triassic sandstones and claystones that underlie the

104 thick Late Jurassic carbonate succession crop out in the south-western part of the catchment

105 (Figure 2). Additional sandstone and claystone lithologies of the same Triassic sequence also

106 appear in the eastern part of the main basin, in subcatchments of the tributaries Truppach and

107 Puettlach. Here, the sandstones and claystones were lifted to the surface along a northwest-

108 southeast striking fault.

109   The vegetation in the south-western part of the catchment is characterized by broad-

110 leaved forest dominated by beeches and scattered small fruit orchards. Coniferous trees

111 largely forest the northern and central parts of the catchment, while the eastern regions consist

112 of grassland pastures. Numerous small villages are present in the basin and, especially in the

113 downstream part of the catchment, agriculture and tourism play an important role in land use

114 (Figure 3). In particular, farming activities along the river course were expected to

115 significantly influence the water chemistry. For information on land cover and land use along

116 the river course refer to Figure 3 and also the high resolution local Riparian Zone (RZ) and

117   Pan-European CORINE Land Cover (CLC) maps of the Copernicus Land Monitoring

118   Service[1] (part of the European Union's Earth Observation Programme).

119   **METHODS**

120   Eight locations along the Wiesent River main course (sites 1 to 8 in Figure 1; exact

121   Global Positioning System coordinates of sampling locations are available in the

122   Supplementary Material) were sampled during eight field campaigns in February, March,

123   April, May, July, August, September, and November 2010 in order to encompass all seasons.

124   Additionally, the six most important tributaries were sampled (sites 9 to 14 in Figure 1).

125   These tributaries were included in the regular sampling interval in April 2010 and sampled

126   during the last six of the eight sampling campaigns. All tributaries were sampled near their

127   confluences with the Wiesent River, with water samples collected manually from the middle

128   of the rivers. All bottles were rinsed several times with sample water before filling. Samples

129   destined for major ion analyses were filled without headspace in double closure 100 mL high-

130   density polyethylene bottles with an inner stopper (product item LR100-2, Gosselin SAS,

131   Borre, France). These were then stored in the dark and at 4°C until analysis.

132   Measurements of temperature, pH, electrical conductivity (EC), and dissolved oxygen

133   (DO) were conducted in the field by a multi-parameter instrument (WTW Multi 350i, WTW

134   GmbH, Weilheim, Germany) during all field campaigns. All probes were calibrated prior to

135   each field campaign. The pH and conductivity probes used built-in automatic temperature

136   compensation functions, and temperature precision is quoted as ± 0.1 °C by the manufacturer.

137   Conductivity values were referenced to 25 °C by a non-linear correction function (nLF) for

---

[1] https://land.copernicus.eu (last accessed 17 January 2018)

138 natural waters. For pH measurements precision was better than $\pm$ 0.05 pH units (1σ) and for

139 conductivity determinations it was better than $\pm$ 5 μS cm^{-1}. Dissolved oxygen was determined

140 by a galvanic sensor and automatically corrected for ambient air pressure by a built-in

141 pressure sensor.

142 　　　Total alkalinity (TA) was determined from 100 mL water samples directly in the field

143 by a Hach Digital Titrator (Model 1690001, Hach Company, Loveland, CO, USA). The

144 titration endpoint was determined by color changes in a pH indicator (bromcresol green-

145 methyl red). At a pH < 9, hydroxide (OH^{-}) does not contribute to TA at an appreciable

146 concentration and other TA contributing species (BOH_4^-, $H_3SiO_4^-$) can be regarded as

147 negligible in the waters examined by this study. Therefore, TA essentially contains only

148 carbonic alkalinity and the titration value was used for the calculation of carbonate species

149 concentrations, which is mainly hydrogencarbonate (HCO_3^-) in the observed pH range (see

150 Verma *et al.*, 2015).

151 　　　Cations (Na^+, K^+, Li^+, NH_4^+, Ca^{2+}, Mg^{2+}) and anions (F^-, Cl^-, NO_3^-, NO_2^-, SO_4^{2-},

152 PO_4^{3-}) were determined by ion chromatography (ICS 2000, Thermo Dionex, Sunnyvale, CA,

153 USA). Prior to ion chromatographic analyses, samples were filtered with 0.45 μm disk filters,

154 which were flushed with sample before the autosampler vials were filled. Limit of

155 quantification (LOQ) for major ions was 0.1 mg L^{-1} with a typical precision of <5% (1σ)

156 relative standard deviation (RSD) based on the repeated analysis of two control standards

157 treated as unknowns in the lower and upper calibration range. Typical charge errors derived

158 from equivalent concentrations of ion chromatography and field titration data were between 5

159 and 12%.

160   **RESULTS**

161   Major ion concentrations (Na^+, K^+, Ca^{2+}, Mg^{2+}, HCO_3^-, Cl^-, NO_3^-, SO_4^{2-}) and

162   measured physico-chemical *in-situ* parameters (temperature, electric conductivity) along the

163   river course are shown in Figure 4. The Supporting Information to this article contains

164   detailed analytical data of the Wiesent River main course (Table S1) and its tributaries (Table

165   S2). The Supporting Material to this article is accessible through the journals website and is

166   additionally archived in the World Data Center PANGAEA[2] for long-term storage and free

167   access. In addition to the ion concentrations and field parameters presented in this article, the

168   stable isotope geochemistry ($\delta^{18}O_{H_2O}$, $\delta^2H_{H_2O}$, and $\delta^{13}C_{DIC}$) of the Wiesent River was also

169   measured and is described in van Geldern *et al.* (2015).

170   The water temperature at the Wiesent River's source was stable during all seasons

171   with an average temperature of (9.0±0.2) °C (arithmetic average ±1 σ). Other parameters,

172   such as pH or conductivity also showed very stable values at the source independent of the

173   season (Figure 4, Table S1). Along the Wiesent River's course, the water temperature

174   correlated with seasonal air temperatures with cooler temperatures in February and March and

175   warmer ones in July and August. Electrical conductivity generally decreased over the first 30

176   km from a value of (728±11) µS/cm at the source to values between 550 to 650 µS/cm. After

177   30 km, the values remained relatively stable and no significant changes were observed over

178   the second half of the river course. Lowest conductivity values were observed during

179   November, March, and August sampling campaigns conducted shortly after precipitation

---

[2] https://doi.pangaea.de/10.1594/PANGAEA.885224

180   events. In contrast, the highest conductivity values were measured in February after a dry

181   period with snow covered landscape and low discharge values. Precipitation and discharge

182   data for the sampling campaigns are published in van Geldern *et al.* (2015).

183   Calcium (Ca^{2+}), showed the highest concentrations amongst all cations, followed by

184   magnesium (Mg^{2+}), sodium (Na^+), and potassium (K^+). Lithium (Li^+) concentrations were

185   always below LOQ (<0.1 mg L^{-1}). Ammonium (NH_4^+) was detected in only two samples

186   during February, with values of 0.11 and 0.28 mg L^{-1}, and was not detectable (below limit of

187   detection, LOD) in all others. In contrast to most other parameters, Ca^{2+} and Mg^{2+}

188   concentrations showed little variability at the source during the various sampling campaigns,

189   although their general downstream patterns were almost identical for all sampling campaigns.

190   Ca^{2+} exhibited a range of 90 to 145 mg L^{-1}, whereas Mg^{2+} concentrations ranged between 15

191   and 45 mg L^{-1} (Figure 4).

192   The concentration pattern of Ca^{2+} showed an initial decrease between the source and

193   sampling site 2 (Wiesentfels; Figure 1), whereas Mg^{2+} increased within the same direction.

194   Further downstream, Ca^{2+} concentrations remained fairly stable and ranged between 105 and

195   130 mg L^{-1}, with exception of the November campaign that was characterized by lower

196   values further downstream. After the initial rise, Mg^{2+} concentrations tended to decrease until

197   sampling site 4 (Waischenfeld) and showed only minor variations thereafter. In particular,

198   Mg^{2+} concentrations showed a clear correlation with corresponding EC values for different

199   sampling campaigns, which in turn were correlated with precipitation events and resulting

200   increased discharge values (data shown in van Geldern *et al.*, 2015). This trend was also

201   obvious to a lesser extent for Ca^{2+}, especially during the November campaign.

202   Na$^+$ concentrations ranged from 8 to 15 mg L^{-1}, stabilizing at a value of (11.2 ± 0.6) mg L^{-1} at

203   the source followed by a slight initial rise. Values declined further downstream to

204   concentrations of about 8 mg L^{-1} at the lower river course.

205   K$^+$ concentrations increased from (1.04 ± 0.24) mg L^{-1} at the source to values of

206   around 2.0 mg L^{-1} downriver. Maximum values of 3.5 mg L^{-1} were recorded during the

207   November sampling campaign at site 4 (Waischenfeld) and also at locations further

208   downstream. Note that during this campaign most other parameters, for example Ca^{2+} and

209   Mg^{2+} concentrations or EC, showed lower values. This trend was most likely related to heavy

210   rains occurring prior to that campaign.

211   The ranking of anions in order of decreasing concentrations at the Wiesent River

212   source was hydrogencarbonate (HCO$_3^-$), nitrate (NO$_3^-$), chloride (Cl$^-$), and sulfate (SO$_4^{2-}$)

213   with concentrations of (357 ± 7), (29.6 ± 2.7), (22.7 ± 1.6), and (15.8 ± 1.5) mg L^{-1},

214   respectively. Interestingly, the downstream behavior revealed different patterns for these

215   anions. NO$_3^-$ showed an almost linear monotonic decline over the river course to (17.6 ± 1.6)

216   mg L^{-1} at the final sampling site 8 (Kirchehrenbach) and HCO$_3^-$ decreased to an average of

217   (307 ± 22) mg L^{-1}. The lowest HCO$_3^-$ values were measured along the lower course during

218   the November sampling campaign. A pronounced decrease was observed after the confluence

219   with the tributary Truppach (10), whereby HCO$_3^-$ concentrations dropped below 250 mg L^{-1}

220   in November. The minimum concentration of 228 mg L^{-1} was recorded at Goessweinstein (6),

221   located downstream of the Puettlach (12) tributary. During other campaigns, HCO$_3^-$

222   concentrations along the lower course (site 4 and downstream), ranged from 340 to 280 mg L$^-$

223   ^{1} (Figure 4).

224   The Cl$^-$ downstream evolution was similar to Na$^+$ or Mg^{2+}, with a distinct increase

225   from the Wiesent source at Steinfeld (1) to Wiesenetfels (2) and subsequently decreasing

226   values. Cl^- concentrations along the lower course ranged from 15 to 25 mg L^{-1} (Figure 4). In

227   contrast, SO_4^{2-} behaved similar to K^+ with a continuous increase along the Wiesent River up

228   to values of 20 to 30 mg L^{-1} near the mouth of the Wiesent at its confluence with the Regnitz.

229   A larger variability of SO_4^{2-} could be observed downstream of sampling site 4

230   (Waischenfeld). Here, maximum concentrations of up to 42 mg L^{-1} were recorded during the

231   November sampling campaign. However, an exception from this behavior was observed in

232   February, when the second highest SO_4^{2-} concentrations were measured at the middle and

233   lower course, while the downstream conductivity curve showed maximum values (Figure 4).

234   Low concentrations for fluoride (F^-) and phosphate (PO_4^{3-}) above LOD were detected

235   in 12 and 11 out of 64 analyses, respectively (cf. Table S1 in Suppl. Material). When

236   detected, typical concentrations of F^- and PO_4^{3-} were below 0.3 mg L^{-1} and never exceeded

237   0.5 mg L^{-1}. Nitrite (NO_2^-) was not detected in any of the sampling campaigns in the main

238   stem of the Wiesent River (cf. Suppl. Material).

239   The tributary and Wiesent River samples are characterized by their major ions in a

240   Piper diagram (Piper, 1944) (Figure 5). Here the tributaries are marked with their numbers in

241   brackets according to Figure 1. The tributaries Kainach (9), Aufsess (11), and Trubach (14)

242   were largely similar to the water chemistry of the main stem of the Wiesent River. The only

243   exception was the Leinleiter tributary (13) with its lower Mg^{2+} concentrations, but most other

244   major ion concentrations were similar to those observed in the main river. Note that the two

245   eastern tributaries Truppach (10) and Puettlach (12) plot differently in Figure 5. For instance,

246   Mg^{2+} concentrations were below 12 mg L^{-1} in all samples taken from the Truppach (10)

247   tributary. Morover, both the Truppach (10) and the Puettlach (12) were characterized by lower

248   HCO_3^-, increased K^+, and high SO_4^{2-} concentrations. These patterns were also seen in the

249 middle and lower course of the Wiesent River. This was particularly evident after

250 precipitation events, for instance during November. Finally, low concentrations of PO_4^{3-} (0.11

251 to 0.72 mg L^{-1}) were found during all campaigns in the Truppach (10) and Puettlach (12), but

252 not in the other tributaries (Table S2).

253 **DISCUSSION**

254 *Geological and anthropogenic controls*

255   The downstream evolution of the parameters discussed above indicates that

256 groundwater is one of the major contributors to the Wiesent River and its tributaries (Figure

257 4). The expectation is that groundwater infiltration to the river occurs primarily by the piston-

258 flow effect, which is then modified along the river course by mixing with tributary-derived

259 water and minor contributions from surface runoff or soil water. Subsurface groundwater

260 contributions to the river and its tributaries are not expected to significantly modify the water

261 chemistry of the main course, as groundwater along the length of the Wiesent River and from

262 most subcatchments originates from the same large deep karst aquifer that feeds the Wiesent

263 River's source (Figure 1). For subcatchments with large proportions of non-carbonate

264 lithology this situation may differ. Increased surface runoff is normally observed during

265 snowmelt and more intensive precipitation events (Bukaveckas, 2010). This would

266 particularly hold true for precipitation in tributaries that drain poorly permeable sediments,

267 such as in the eastern part of the catchment (Truppach (10) and Puettlach (12)). In these

268 subcatchments, which are dominated by clay and sandstone-claystone lithologies, overland

269 flow generation should play a more important role than in permeable karst lithology with its

270 fast infiltration rates (Bakalowicz, 2005; Ford and Williams, 2007). The rapid delivery of

271 low-mineralized rain water via overland flow and shallow soil flowpaths results in lower

272   solute concentrations during increased discharge (Allan and Castillo, 2007; Bukaveckas,

273   2010). Mixing of these tributary waters with the main river stem is the most important process

274   affecting the dilution of total dissolved solids (TDS), as indicated by lower EC values.

275   When tributaries are chemically different as compared to the main stem of the Wiesent

276   River, their influences are expected to be obvious. For instance, lower Mg^{2+} concentrations in

277   the Truppach (10; Table S2) likely caused the pronounced drop in Mg^{2+} after sampling sites 3

278   (Hollfeld) in the Wiesent River (Figure 4). This decline was even more pronounced during

279   periods of low conductivity following precipitation events.

280   On the other hand, contributions of tributaries that drain a similar lithology as the

281   Wiesent River are harder to detect by changes in aquatic chemistry and natural environmental

282   tracers (Clark and Fritz, 1997; Cook and Herczeg, 2000). For instance, near the catchment

283   outlet, the lithology along the Wiesent River valley changes from carbonate rocks to

284   claystone. The formation is known as the Feuerletten Formation from the Late Trassic period.

285   With exception of small changes in Ca^{2+}, Mg^{2+}, and Na^+, the measured parameters did not

286   respond to this prominent change in riverbed lithology. This indicates that groundwater

287   contributions at the final river stretch likely become less important due to the less permeable

288   nature of the underlying thick claystone formation.

289   At the source of the Wiesent, Ca^{2+}, Mg^{2+}, and HCO_3^- account for 86 % of the TDS and

290   along the river course, this value varies only slightly between 81 and 88 %. This shows that

291   carbonate weathering of calcite ($CaCO_3$) and dolomite ($CaMg(CO_3)_2$) mainly accounts for the

292   high concentrations of these three ions. The stoichiometry of carbonate weathering reactions

293   demands that carbonate-derived Ca^{2+} and Mg^{2+} should be equal to that of HCO_3^- when

294   expressed in (milli)equivalents per liter (meq L^{-1}). Such a plot of ($Ca^{2+} + Mg^{2+}$) over HCO_3^-

295   concentrations reveals a general excess of Ca^{2+} and Mg^{2+} over HCO_3^- (Figure 6A). This

14

296   excess of cations is partially balanced by Cl^-, SO_4^{2-}, and NO_3^-, and suggests that fractions of

297   Ca^{2+}or Mg^{2+} concentrations in the watershed were not exclusively derived from carbonate

298   weathering (Meybeck, 1987). Other potential natural sources of Ca^{2+} are gypsum or the

299   silicate weathering of Ca-bearing minerals such as anorthite (Berner *et al.*, 1983; Meybeck,

300   1987). However, both minerals are of minor importance in the Jurassic limestone formations

301   and are therefore unlikely candidates for leaching Ca^{2+} and Mg^{2+}.

302   Other sources for this excess include primary (N, P, K) and secondary (Ca, Mg, S)

303   nutrient mineral fertilizers that contain Ca^{2+} or Mg^{2+}-bearing compounds, such as for example

304   magnesium ammonium phosphate (MAP) (EPA, 1999). This should also correlate with other

305   solutes that are typically derived from these fertilizers, such as NO_3^-. Further anthropogenic

306   sources that may exist in the watershed include organic fertilizers or domestic sewage.

307   Typical anthropogenic compounds are PO_4^{3-}, SO_4^{2-} and nitrogen (N) compounds (NO_3^-, NO_2^-,

308   NH_4^+) sourced from manure and mineral fertilizers. In particular, elevated NO_3^-

309   concentrations are often related to the use of such fertilizers. During this study, the highest

310   concentrations of NO_3^- were found at the source of the Wiesent River with a consistent value

311   of (29.6 ± 2.7) mg L^{-1}. This stability of NO_3^- concentrations at the source suggests that NO_3^-

312   may have been continuously transferred into the feeding karst aquifer, which acted as a large

313   reservoir (see also van Geldern *et al.*, 2015 for additional information). With respect to the

314   common dual-flow concept for groundwater flow in karst aquifers (Atkinson, 1977; White,

315   1988; Ford and Williams, 1989; Kiraly, 1998; Ford and Williams, 2007; Goldscheider and

316   Drew, 2007), the observed pattern at the Wiesent source reflects the diffusive flow component

317   through fractures and pores. In contrast to the faster reacting conduit flow system that

318   transports water along pipe-like conduits and cave stream channel, the diffusive flow reflects

319   NO_3^- average values and long-term-trends (Huebsch *et al.*, 2014). Subsequently, NO_3^- likely

320   has accumulated over decades in the deep karst aquifer and seasonal variations became

321   negligible.

322   This supports the interpretation that the observed excess of Ca^{2+} and Mg^{2+} is a result of

323   long-term anthropogenic influences on the groundwater, particularly at the Wiesent River

324   spring and the upper reaches. It is therefore indicative of influences from farming activities in

325   the upper part of the catchment. The Wiesent River has its source in a rural, largely natural

326   region where forests and grassland dominate large portions of the catchment and industry

327   does not play a significant role (Figure 3). Therefore, anthropogenic signals in river water

328   chemistry were expected to be minimal, with inorganic aquatic chemistry mainly mirroring

329   weathering processes or changes in lithology. However, particularly in karst systems, virtually

330   unfiltered anthropogenic influences may directly enter the source and the river via the fast

331   conduit and the slower diffusive flow systems (Atkinson, 1977; Ford and Williams, 2007).

332   As opposed to the expected trend of increasing NO_3^- concentrations further

333   downstream where agriculture and urbanization is more prevalent, a contrary pattern was

334   observed: NO_3^- concentrations were found to be highest at the source of the Wiesent River

335   (see discussion above) and subsequently decreased with distance from the headwaters during

336   all sampling periods (Figure 4). This pattern is further suggestive of the long-term influences

337   of agricultural land use on groundwater, particularly in the upstream section of the watershed.

338   Even though agricultural activities are also prevalent in the downstream part of the catchment,

339   their associated NO_3^- releases may not reach the river as quickly because the lithology

340   contains a high proportion of fine sandstones and shales (Figure 1) that slows or hampers

341   groundwater-related transport to the river. During large precipitation events, solutes can be

342   mobilized and transported to the river course quickly by overland flow and shallow soil flow

343   paths, but short transit times along these paths limit the interaction between low-mineralized

344   rainwater and soil. High discharge is therefore often characterized by lower concentrations of

345   dissolved substances (Bukaveckas, 2010). Such patterns can be identified in our data set, for

346   example during the sampling campaigns in March, August, and November (Figure 4). These

347   sampling campaigns were conducted shortly after precipitation events (see above) and are

348   characterized by low EC values.

349   As for other anthropogenic parameters, road salt and domestic sewage are a primary

350   source of Na^+ and especially Cl^- (Liu *et al.*, 2008; Sun *et al.*, 2014) since natural sources,

351   such as evaporite dissolution or atmospheric sea salt deposition (Meybeck, 1987) is unlikely

352   in the study area. Increases in Na^+ or Cl^- concentrations were not observed at the source

353   during colder periods. This could indicate that either they were dampened in the large feeding

354   karst reservoir or that road salting had only a minor influence on the river water chemistry.

355   Since both Cl^- and Na^+ showed no distinct seasonality over the entire course or the river, a

356   pronounced influence of this source is likely minor in this catchment. It is more likely that

357   these elements reach the river via agricultural activities that are more dominant in the source

358   region, as previously stated. At this juncture, it is unclear why both Cl^- and Na^+ show

359   significant increases from the spring to the second sampling station (site 2, Wiesentfels),

360   although this trend may be related to the presence of point sources such as sewage discharge

361   or livestock waste from farms (Mullaney *et al.*, 2009; Kelly *et al.*, 2012).

362   Cl^- was also found to be in excess of Na^+ and K^+ and their inclusion in a cation-anion

363   plot does not follow a 1:1 ratio (Figure 6B). The Cl^- excess could in part be balanced by

364   excess Ca^{2+} and Mg^{2+} that does not account for carbonate weathering. When assuming that

365   this cation excess stems from fertilizer use in the upstream part of the catchment, it supports

366   the hypothesis that fertilizers are more pronounced in upstream river sections and may have

367   entered the river via diffusive flow in the present karst system (Huebsch *et al.*, 2014).

368   Other potash (K_2O) bearing fertilizers with compounds such as KCl or K_2SO_4 may

369   also have contributed to the fertilizer load of the river. However, both K^+ and SO_4^{2-} exhibit

370   their lowest values in the source region and show increases further downstream (Figure 4). At

371   a glance, this pattern does not appear to support the hypothesis of more pronounced fertilizer

372   input in the upstream part of the catchment. However, it is possible that both ions enter the

373   river as a result of fertilizer transport in the upstream, karst-dominated section of the

374   catchment. The baseline values at the source may then have increased further downstream

375   mainly as a result of K^+ and SO_4^{2-} released from weathering processes in the clay-rich shale

376   formations in the eastern subcatchments, and discharged into the main river stem via

377   tributaries. These and other mechanisms of tributary influences are discussed below.

378   *Downstream geochemical evolution*

379   After setting of the initial values for physico-chemical parameters at the source, many

380   parameters show changes along the river course. This may be either related to processes that

381   occur within the main river itself such as seasonal temperature changes, or is due to the inflow

382   and mixing of waters from different sources (Allan and Castillo, 2007; Likens, 2010).

383   An important question in river research is the interaction between river water and

384   surface water within the hyporheic and riparian zones along the river course (Krause *et al.*,

385   2009; Kanduč *et al.*, 2012; Kanduč *et al.*, 2013; Krause *et al.*, 2014). Depending on the

386   hydraulic system, the river can lose water to groundwater via outflow through the riverbed

387   (Winter *et al.*, 1998; Engelhardt *et al.*, 2014). This situation is denoted as a losing stream.

388   Alternatively, water from the riparian zone can feed the river, which is denoted as a gaining

389   steam. Different environmental tracers, for example temperature, stable isotopes, or

390   wastewater-related pollutants, have been used to investigate these interactions in detail

391   (Engelhardt *et al.*, 2014; Fox *et al.*, 2016). Furthermore, tributaries with differing water

392   chemistry that mix with the main river course can also induce changes in water chemistry

393   when these differences and fluxes are large enough to cause a measurable shift (Perrin *et al.*,

394   2007; Torres *et al.*, 2017).

395   The downstream temperature development of the Wiesent River varies seasonally,

396   with higher temperatures in summer and lower temperatures in winter (Figure 4).

397   Groundwater seeps would shift the warm or cold temperature curve locally towards the

398   average groundwater temperature of about 9 ° C for this region. However, the spatial

399   resolution along the river is not detailed enough to detect point-source groundwater inflow.

400   This is because groundwater temperature can be expected to adjust quickly to the river water

401   temperature. Minor groundwater contributions would therefore only be detectable close to the

402   point of inflow. However, a steady and spatially ubiquitous groundwater inflow along the

403   entire river course would likely dampen seasonal changes within the river. Such trends could

404   only be observed at the source and for the remainder of the river length it is more likely that

405   groundwater contributions are of minor importance.

406   A closer examination of the downstream curves showed a notable increase in Mg^{2+}

407   concentrations of 7 to 13 mg L^{-1} from the source to sampling site 2 (Wiesentfels; Figure 4). A

408   larger fraction of dolomite weathering might have increased the portion of Mg^{2+} over Ca^{2+}.

409   However, this shift was also correlated with increases of Na^+ and Cl^- (Figure 4). To a large

410   degree, the latter elements are likely of anthropogenic origin (Jiang *et al.*, 2009) and this

411   coincidence suggests that the Mg^{2+} increase has a potential (but as yet unidentified)

412   anthropogenic component. This is supported by the fact that the increase in Cl^- was larger

413   than the corresponding increase in Na^+, so Cl^- could have contributed to the buffering of the

414   Mg^{2+} increase. However, even when accounting for Cl^-, a negative charge deficit persisted

415   and Mg^{2+} must have been additionally balanced by other anions. As no other major anions

19

416   (SO_4^{2-}, NO_3^-) showed a corresponding increase, the surplus of Mg^{2+} is most likely buffered by

417   organic compounds that were not measured in this study.

418   The downstream evolution of K^+ and SO_4^{2-} in the Wiesent River showed opposing

419   patterns as compared to the other major ions along the course (see above). Both ion

420   concentrations gradually increased downstream, whereas other major ion concentrations

421   decreased most likely due to dilution effects by the tributaries Truppach (10) and Puettlach

422   (12), which drain a different lithology. Their lithology is dominated by claystone and

423   sandstone (see Figure 1) and increased concentrations of K^+ and SO_4^{2-} were observed in these

424   two eastern tributaries (Table S2 in Supplementary Material). A potential anthropogenic

425   source are fertilizers because potassium (K) is, together with nitrogen (N) and phosphorous

426   (P), a primary nutrient (macronutrient) and component in many commercial NPK fertilizers

427   (EPA, 1999). Potassium Sulfate (K_2SO_4) is a common inorganic fertilizer that is often used in

428   fruit orchards. K^+ and SO_4^{2-} show a fairly strong correlation in the two subcatchments

429   (Pearson correlation coefficient $r = 0.69$, $p = 0.012$ for a two tailed test; statistically

430   significant at the $> 95\%$ level) but only about one-tenth of the SO_4^{2-} is balanced by K^+ in this

431   scenario. Other common K-bearing fertilizers are KCl, KNO_3, and the crude potassium salts

432   sylvinite and kainite.

433   Alternatively, one plausible natural source for K^+ is weathering of orthoclase and other

434   K-bearing silicate minerals in the clastic sediments (Wollast and Mackenzie, 1983; Struyf *et*

435   *al.*, 2009). As a result of these weathering processes, a larger amount of K^+ may have been

436   transported into the Wiesent River.

437   The higher SO_4^{2-} concentrations could have been caused by the dissolution of gypsum

438   and/or weathering of pyrite (Sun *et al.*, 2014). Both minerals are present in the Lower and

439   Middle Jurrasic formations (Krumbeck, 1956; Schröder, 1968) and pyrite is especially

440   abundant in the thick claystone sequence of the 'Amaltheenton' and 'Opalinuston' formations

441   that cover large areas of the eastern subcatchments (Wippern, 1955). The principles of pyrite

442   oxidation follow a sequence of reactions that involve microbiologically-mediated and oxic

443   decomposition of pyrite followed by an anoxic decomposition of pyrite by ferric iron

444   (Lowson, 1982; Evangelou, 1995). The overall stoichiometry is represented by:

$$2FeS_2 + 7O_2 + 2H_2O \rightarrow 2Fe^+ + 4SO_4^{2-} + 4H^+ \tag{1}$$
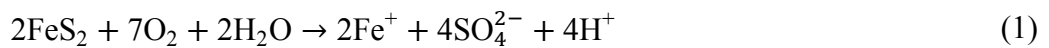
445   Pyrite weathering reactions release acidity and result in low pH values. However, lower pH

446   values were neither observed in the Wiesent nor in any of the tributaries (cf. Tables S1 and S2

447   and van Geldern *et al.*, 2015). This absence of an expected pH decrease could be explained

448   by the presence of up to 10% carbonates in the claystones (Schröder, 1968). This means that

449   acidity derived from equation (1) could become directly neutralized by reaction with

450   carbonates.

451   Unexpectedly higher concentrations of K^+ and SO_4^{2-} in the Truppach (10) and

452   Puettlach (12) tributaries was observed in November: samples from this month showed

453   increased concentrations of K^+ and SO_4^{2-} that were also found in the middle and lower

454   reaches of the Wiesent River, downstream of the Truppach (10) and Puettlach (12)

455   confluences (Figure 4). In contrast, most other ions (e.g., Ca^{2+} or Mg^{2+}) were diluted. This

456   dilution can be attributed to increased fluxes of low-mineralized surface runoff following a

457   heavier period of rainfall in November (see van Geldern *et al.*, 2015 for precipitation and

458   discharge data). Surface runoff was also expected to dilute concentrations of K^+ and SO_4^{2-}.

459   However, the data suggest that both ions were mobilized within the soil zone and flushed out,

460   with increased concentrations along the eastern tributaries into the Wiesent River during

461   precipitation events (van Geldern *et al.*, 2015).

462 **CONCLUSIONS**

463   The Wiesent River has an unusual chemical downriver evolution, particularly for

464 solutes that are often derived from agricultural fertilizers. While increased anthropogenic

465 activities normally occur in the downriver sections of the catchment, an unexpectedly stronger

466 fertilizer-derived signal (particularly NO_3^-) was discerned in its upstream area. These

467 agricultural inputs may have been introduced through fast conduit and fracture flow in the

468 karst lithology of the upstream catchment. Agricultural influences may even stem from

469 beyond the catchment surface water boundaries. After leaving the source, these inputs became

470 diluted further downstream, specifically via tributaries that were not sourced from carbonate

471 lithologies. While Ca^{2+}, HCO_3^- and NO_3^- decreased over the course of the river, we found

472 increases of K^+ and SO_4^{2-} in the downstream section that is more influenced by clay

473 lithologies. This enables a division of the river into two sections: an upstream part that is

474 dominated by karst and receives strong fertilizer inputs, and a downstream section that

475 receives less groundwater inputs but is subject to increased contributions by tributaries that

476 drain sandstone and shale lithologies. This highlights the importance of including tributaries

477 in river studies.

478   This study was limited to the year 2010 and it raises a question about the long-term

479 evolution of anthropogenic related contamination, for example by NO_3^-. The Bavarian

480 Environmental Agency (Landesamt für Umwelt - LfU) operates a long-term monitoring

481 station for basic river water chemistry near our lower-course sampling point Kirchehrenbach

482 (8) (Figure 1). The mean annual average NO_3^- concentrations for the period from 1985 to

483 2015 are shown in Table 1. The average values remained almost unchanged with an average

484 value of (19.5 ± 1.0) mg L^{-1}. A minor tendency to somewhat lower values can observed since

485 ~2008, but overall the long-term data set indicates that our study is representative not only for

486 2010, but also for any given period of time.

487   A valuable tool for future studies assessing the natural or anthropogenic origin of

488 solute compounds, such as NO_3^-, SO_4^{2-} or Cl^-, are light stable isotope analyses of the

489 elements C, H, O, N, S (e.g., Michalski *et al.*, 2004; Bateman and Kelly, 2007; Liu *et al.*,

490 2008; Widory *et al.*, 2013; Amiri *et al.*, 2015; Michalski *et al.*, 2015). In addition, future

491 studies should include ecological indicators that may be more sensitive to fertilizer input, such

492 as counts of specific organisms and quantification of sediment loads.

493   Overall, our findings indicate that bedrock geology remains the dominant control on

494 the major ion chemistry of the Wiesent River, and that agricultural influences are the

495 strongest near the headwaters despite increased land-use further downstream, due to long-

496 term storage and accumulation in karst aquifers. This feature may not be unique to the

497 Wiesent River system, and subsequent work in other river systems could establish whether

498 such patterns are ubiquitous worldwide.

499   Carbonate outcrops for Europe and the entire world are estimated with 22% and 13%,

500 respectively (Williams and Ford, 2006; Hollingsworth, 2009; Williams and Fong, 2010),

501 illustrating the global significance of karst. In karst regions, the source spring is the most

502 important locale to obtain information about the functioning of the entire watershed system

503 (Bakalowicz, 2005). Understanding the hydro-chemical pattern of rivers from their sources to

504 lower reaches will facilitate freshwater security, ecosystem health, and the sustainability of

505 drinking water resources.

514

515 **APPENDIX**

516 Supplementary Material to this article is available at https://doi.org/10.1002/hyp.11461 and

517 from PANGAEA (www.pangaea.de) at https://doi.pangaea.de/10.1594/PANGAEA.885224.

518

519 **References**

520 Allan JD, Castillo MM. 2007. *Stream Ecology - Structure and function of running water*. 2nd

521   Edn., Springer; 445.

522 Amiri H, Zare M, Widory D. 2015. Assessing sources of nitrate contamination in the Shiraz

523   urban aquifer (Iran) using the δ^{15}N and δ^{18}O dual-isotope approach. *Isotopes in*

524   *Environmental and Health Studies* **51**: 392-410. DOI:

525   10.1080/10256016.2015.1032960.

526 Apel R, Büttner G. 1995. *Nördliche Frankenalb - Hydrogeologie*. Bayerisches Geologisches

527   Landesamt (GLA); 119.

528 Atkinson TC. 1977. Diffuse flow and conduit flow in limestone terrain in the Mendip Hills,

529   Somerset (Great Britain). *Journal of Hydrology* **35**: 93-110. DOI: 10.1016/0022-

530   1694(77)90079-8.

531 Aucour A-M, Sheppard SMF, Guyomar O, Wattelet J. 1999. Use of ^{13}C to trace origin and

532   cycling of inorganic carbon in the Rhône river system. *Chemical Geology* **159**: 87-

533   105. DOI: 10.1016/S0009-2541(99)00035-2.

534 Aufdenkampe AK, Mayorga E, Raymond PA, Melack JM, Doney SC, Alin SR, Aalto RE,

535   Yoo K. 2011. Riverine coupling of biogeochemical cycles between land, oceans, and

536   atmosphere. *Frontiers in Ecology and the Environment* **9**: 53-60. DOI:

537   10.1890/100014.

538 Bakalowicz M. 2005. Karst groundwater: a challenge for new resources. *Hydrogeology*

539   *Journal* **13**: 148-160. DOI: 10.1007/s10040-004-0402-9.

540 Barth JAC, Cronin AA, Dunlop J, Kalin RM. 2003. Influence of carbonates on the riverine

541   carbon cycle in an anthropogenically dominated catchment basin: Evidence from

542   major elements and stable carbon isotopes in the Lagan River (N. Ireland). *Chemical*

543   *Geology* **200**: 203-216.

544 Bateman AS, Kelly SD. 2007. Fertilizer nitrogen isotope signatures. *Isotopes in*

545   *Environmental and Health Studies* **43**: 237-247. DOI: 10.1080/10256010701550732.

546 Berner RA, Lasaga AC, Garrels RM. 1983. The carbonate-silicate geochemical cycle and its

547   effect on atmospheric carbon dioxide over the past 100 million years. *American*

548   *Journal of Science* **283**: 641-683.

549 Biggs TW, Dunne T, Domingues TF, Martinelli LA. 2002. Relative influence of natural

550   watershed properties and human disturbance on stream solute concentrations in the

551   southwestern Brazilian Amazon basin. *Water Resources Research* **38**: 25-21-25-16.

552   DOI: 10.1029/2001WR000271.

553 Brunet F, Potot C, Probst A, Probst JL. 2011. Stable carbon isotope evidence for nitrogenous

554   fertilizer impact on carbonate weathering in a small agricultural watershed. *Rapid*

555   *Communications in Mass Spectrometry* **25**: 2682-2690. DOI: 10.1002/rcm.5050.

556 Bukaveckas PA. 2010. Hydrology: Rivers. In: *River Ecosystem Ecology: A Global*

557   *Perspective*, Likens GE (ed.) Academic Press, pp: 32-44.

558 Cartwright I. 2010. The origins and behaviour of carbon in a major semi-arid river, the

559   Murray River, Australia, as constrained by carbon isotopes and hydrochemistry.

560   *Applied Geochemistry* **25**: 1734-1745. DOI: 10.1016/j.apgeochem.2010.08.020.

561 Chetelat B, Liu CQ, Zhao ZQ, Wang QL, Li SL, Li J, Wang BL. 2008. Geochemistry of the

562   dissolved load of the Changjiang Basin rivers: Anthropogenic impacts and chemical

563   weathering. *Geochimica et Cosmochimica Acta* **72**: 4254-4277. DOI:

564   10.1016/j.gca.2008.06.013.

565   Clark I, Fritz P. 1997. *Environmental Isotopes in Hydrology*. CRC Press, Boca Raton, FL;

566   328.

567   Cook PG, Herczeg AL. 2000. *Environmental Tracers in Subsurface Hydrology*. Springer,

568   New York; 529.

569   Daesslé LW, van Geldern R, Orozco-Durán A, Barth JAC. 2016. The 2014 water release into

570   the arid Colorado River delta and associated water losses by evaporation. *Science of*

571   *the Total Environment* **542**: 586-590. DOI: 10.1016/j.scitotenv.2015.09.157.

572   Daesslé LW, Orozco A, Struck U, Camacho-Ibar VF, van Geldern R, Santamaría-del-Angel

573   E, Barth JAC. 2017. Sources and sinks of nutrients and organic carbon during the

574   2014 pulse flow of the Colorado River into Mexico. *Ecological Engineering* **106**:

575   799-808. DOI: 10.1016/j.ecoleng.2016.02.018.

576   Doctor DH, Kendall C, Sebestyen SD, Shanley JB, Ote N, Boyer EW. 2008. Carbon isotope

577   fractionation of dissolved inorganic carbon (DIC) due to outgassing of carbon

578   dioxide from a headwater stream. *Hydrological Processes* **22**: 2410-2423. DOI:

579   10.1002/hyp.6833.

580   Engelhardt I, Barth JAC, Bol R, Schulz M, Ternes TA, Schüth C, van Geldern R. 2014.

581   Quantification of long-term wastewater fluxes at the surface water/groundwater-

582   interface: An integrative model perspective using stable isotopes and acesulfame.

583   *Science of the Total Environment* **466-467**: 16-25. DOI:

584   10.1016/j.scitotenv.2013.06.092.

585   EPA. 1999. *Background report on fertilzer use, contaminants and regulations*. Office of

586   Pollution Prevention and Toxics, Unites States Environmental Protection Agency

587   (EPA), EPA 747-R-98-003; 121.

588   Evangelou VP. 1995. *Pyrite oxidation and its control*. CRC Press; 293.

589   Flintrop C, Hohlmann B, Jasper T, Korte C, Podlaha OG, Scheele S, Veizer J. 1996. Anatomy

590   of pollution; rivers of North Rhine-Westphalia, Germany. *American Journal of*

591   *Science* **296**: 58-98. DOI: 10.2475/ajs.296.1.58.

592   Ford DC, Williams PW. 1989. *Karst Geomorphology and Hydrogeology*. Chapman and Hall,

593   London; 601.

594   Ford DC, Williams PW. 2007. *Karst Hydrogeology and Geomorphology*. John Wiley & Sons,

595   Chichester; 576.

596   Fox A, Laube G, Schmidt C, Fleckenstein JH, Arnon S. 2016. The effect of losing and

597   gaining flow conditions on hyporheic exchange in heterogeneous streambeds. *Water*

598   *Resources Research* **52**: 7460-7477. DOI: 10.1002/2016WR018677.

599   Gaillardet J, Dupre B, Allegre CJ, Negrel P. 1997. Chemical and physical denudation in the

600   Amazon River basin. *Chemical Geology* **142**: 141-173. DOI: 10.1016/S0009-

601   2541(97)00074-0.

602   Gaillardet J, Dupre B, Louvat P, Allegre CJ. 1999. Global silicate weathering and CO_2

603   consumption rates deduced from the chemistry of large rivers. *Chemical Geology*

604   **159**: 3-30. DOI: 10.1016/S0009-2541(99)00031-5.

605   Galy A, France-Lanord C. 1999. Weathering processes in the Ganges-Brahmaputra basin and

606   the riverine alkalinity budget. *Chemical Geology* **159**: 31-60. DOI: 10.1016/S0009-

607   2541(99)00033-9.

608   Gandois L, Perrin A-S, Probst A. 2011. Impact of nitrogenous fertiliser-induced proton

609   release on cultivated soils with contrasting carbonate contents: A column experiment.

610   *Geochimica et Cosmochimica Acta* **75**: 1185-1198. DOI: 10.1016/j.gca.2010.11.025.

611   Gibbs RJ. 1970. Mechanisms Controlling World Water Chemistry. *Science* **170**: 1088.

612   Gleick PH. 1996. Water resources. In: *Encyclopedia of Climate and Weather*, Schneider SH

613   (ed.) Oxford University Press, New York, pp: 817-823.

614   Goldscheider N, Drew D. 2007. Methods in Karst Hydrogeology. Taylor & Francis, London,

615   pp: 264.

616   Grosbois C, Négrel P, Fouillac C, Grimaud D. 2000. Dissolved load of the Loire River:

617   Chemical and isotopic characterization. *Chemical Geology* **170**: 179-201. DOI:

618   10.1016/S0009-2541(99)00247-8.

619   Hélie J-F, Hillaire-Marcel C, Rondeau B. 2002. Seasonal changes in the sources and fluxes of

620   dissolved inorganic carbon through the St. Lawrence River—isotopic and chemical

621   constraint. *Chemical Geology* **186**: 117-138. DOI: 10.1016/S0009-2541(01)00417-X.

622   Hollingsworth E. 2009. *Karst Regions of the World (KROW)---Populating global karst*

623   *datasets and generating maps to advance the understanding of karst occurrence and*

624   *protection of karst species and habitats worldwide*. University of Arkansas, MSc

625   Science thesis; available online: www.karstportal.org/download/file/fid/244

626   (accessed 31 March 2014); 129.

627   Huebsch M, Fenton O, Horan B, Hennessy D, Richards KG, Jordan P, Goldscheider N,

628   Butscher C, Blum P. 2014. Mobilisation or dilution? Nitrate response of karst springs

629   to high rainfall events. *Hydrology and Earth System Sciences* **18**: 4423-4435. DOI:

630   10.5194/hess-18-4423-2014.

631   Jiang Y, Wu Y, Groves C, Yuan D, Kambesis P. 2009. Natural and anthropogenic factors

632   affecting the groundwater quality in the Nandong karst underground river system in

633   Yunan, China. *Journal of Contaminant Hydrology* **109**: 49-61. DOI:

634   10.1016/j.jconhyd.2009.08.001.

635   Kanduč T, Mori N, Kocman D, Stibilj V, Grassa F. 2012. Hydrogeochemistry of Alpine

636   springs from North Slovenia: Insights from stable isotopes. *Chemical Geology* **300-**

637   **301**: 40-54. DOI: 10.1016/j.chemgeo.2012.01.012.

638   Kanduč T, Šturm MB, McIntosh J. 2013. Chemical Dynamics and Evaluation of

639   Biogeochemical Processes in Alpine River Kamniška Bistrica, North Slovenia.

640   *Aquatic Geochemistry* **19**: 323-346. DOI: 10.1007/s10498-013-9197-4.

641   Kanduč T, Szramek K, Ogrinc N, Walter L. 2007. Origin and cycling of riverine inorganic

642   carbon in the Sava River watershed (Slovenia) inferred from major solutes and stable

643   carbon isotopes. *Biogeochemistry* **86**: 137-154. DOI: 10.1007/s10533-007-9149-4.

644   Kelly WR, Panno SV, Hackley K. 2012. *The Sources, Distribution, and Trends of Chloride in*

645   *the Waters of Illinois*. Illinois State Water Survey, Champaign, IL; 67.

646   Kendall C, Silva SR, Kelly VJ. 2001. Carbon and nitrogen isotopic compositions of

647   particulate organic matter in four large river systems across the United States.

648   *Hydrological Processes* **15**: 1301-1346. DOI: 10.1002/hyp.216.

649   Kiraly L. 1998. Modelling karst aquifers by the combined discrete chan- nel and continuum

650   approach. *Bulletin d'Hydrogéologie* **16**: 77-98. http://doc.rero.ch/record/260628

651   Krause S, Boano F, Cuthbert MO, Fleckenstein JH, Lewandowski J. 2014. Understanding

652   process dynamics at aquifer-surface water interfaces: An introduction to the special

653   section on new modeling approaches and novel experimental technologies. *Water*

654   *Resources Research* **50**: 1847-1855. DOI: 10.1002/2013WR014755.

655   Krause S, Hannah DM, Fleckenstein JH. 2009. Hyporheic hydrology: interactions at the

656   groundwater-surface water interface. *Hydrological Processes* **23**: 2103-2107. DOI:

657   10.1002/hyp.7366.

658   Krumbeck L. 1956. *Erläuterungen zur Geologischen Karte von Bayern 1: 25000 - Blatt Nr.*

659   *6232 Forchheim*. Bayerisches Geologisches Landesamt; 80.

660   Lee K, van Geldern R, Barth JAC. 2017. A high-resolution carbon balance in a temperate

661   catchment: insights from the Schwabach River, Germany. *Applied Geochemistry* **85**:

662   86-96. DOI: 10.1016/j.apgeochem.2017.08.007.

663   LfU. 2014. Hochwassernachrichtendienst. Bayerisches Landesamt für Umwelt (LfU).

664   Accessible at http://www.hnd.bayern.de, (last accessed 28 Feb 2014).

665   Likens GE. 2010. River Ecosystem Ecology: A Global Perspective. Academic Press, San

666   Diego, pp: 424.

667   Liu C-Q, Lang Y-C, Satake H, Wu J, Li S-L. 2008. Identification of Anthropogenic and

668   Natural Inputs of Sulfate and Chloride into the Karstic Ground Water of Guiyang,

669   SW China: Combined $\delta^{37}Cl$ and $\delta^{34}S$ Approach. *Environmental Science &*

670   *Technology* **42**: 5421-5427. DOI: 10.1021/es800380w.

671   Lowson RT. 1982. Aqueous oxidation of pyrite by molecular oxygen. *Chemical Reviews* **82**:

672   461-497. DOI: 10.1021/cr00051a001.

673   Marx A, Dusek J, Jankovec J, Sanda M, Vogel T, van Geldern R, Hartmann J, Barth JAC.

674   2017a. A review of CO_2 and associated carbon dynamics in headwater streams: a

675   global perspective. *Reviews of Geophysics* **55**: 560-585. DOI:

676   10.1002/2016RG000547.

677   Marx A, Hintze S, Sanda M, Jankovec J, Oulehle F, Dusek J, Vitvar T, Vogel T, van Geldern

678   R, Barth JAC. 2017b. Acid rain footprint three decades after peak deposition: Long-

679   term recovery from pollutant sulphate in the Uhlirska catchment (Czech Republic).

680   *Science of the Total Environment* **598**: 1037-1049. DOI:

681   10.1016/j.scitotenv.2017.04.109.

682   Meybeck M. 1982. Carbon, nitrogen, and phosphorus transport by world rivers. *American*

683   *Journal of Science* **282**: 401-450. DOI: 10.2475/ajs.282.4.401.

684   Meybeck M. 1987. Global chemical weathering of surficial rocks estimated from river

685   dissolved loads. *American Journal of Science* **287**: 401-428. DOI:

686   10.2475/ajs.287.5.401.

687   Michalski G, Böhlke JK, Thiemens M. 2004. Long term atmospheric deposition as the source

688   of nitrate and other salts in the Atacama Desert, Chile: New evidence from mass-

689   independent oxygen isotopic compositions. *Geochimica et Cosmochimica Acta* **68**:

690   4023-4038. DOI: 10.1016/j.gca.2004.04.009.

691   Michalski G, Kolanowski M, Riha KM. 2015. Oxygen and nitrogen isotopic composition of

692   nitrate in commercial fertilizers, nitric acid, and reagent salts. *Isotopes in*

693   *Environmental and Health Studies* **51**: 382-391. DOI:

694   10.1080/10256016.2015.1054821.

695   Milliman JD, Farnsworth KL. 2011. *River Discharge to the Coastal Ocean: A Global*

696   *Synthesis*. Cambridge University Press, Cambridge; 392.

697   Mullaney JR, Lorenz DL, Arntson AD. 2009. *Chloride in Groundwater and Surface Water in*

698   *Areas Underlain by the Glacial Aquifer System, Northern United States*. U.S.

699   Geological Survey Scientic Investigations Report 2009–5086; 41.

700   Négrel P, Allègre CJ, Dupré B, Lewin E. 1993. Erosion sources determined by inversion of

701   major and trace element ratios and strontium isotopic ratios in river: The Congo

702   Basin case. *Earth and Planetary Science Letters* **120**: 59-76. DOI: 10.1016/0012-

703   821X(93)90023-3.

704   Perrin A-S, Probst A, Probst J-L. 2008. Impact of nitrogenous fertilizers on carbonate

705   dissolution in small agricultural catchments: Implications for weathering CO2 uptake

706   at regional and global scales. *Geochimica et Cosmochimica Acta* **72**: 3105-3123.

707   DOI: 10.1016/j.gca.2008.04.011.

708   Perrin J, Jeannin PY, Cornaton F. 2007. The role of tributary mixing in chemical variations at

709   a karst spring, Milandre, Switzerland. *Journal of Hydrology* **332**: 158-173. DOI:

710   10.1016/j.jhydrol.2006.06.027.

711   Piper AM. 1944. A graphic procedure in the geochemical interpretation of water analysis.

712   *Transactions American Geophysical Union* **25**: 914-923. DOI:

713   10.1029/TR025i006p00914.

714   Probst A, Viville D, Fritz B, Ambroise B, Dambrine E. 1992. Hydrochemical budgets of a

715   small forested granitic catchment exposed to acid deposition: The strengbach

716   catchment case study (Vosges massif, France). *Water, Air, & Soil Pollution* **62**: 337-

717   347. DOI: 10.1007/BF00480265.

718   Raymond PA, Hartmann J, Lauerwald R, Sobek S, McDonald C, Hoover M, Butman D,

719   Striegl R, Mayorga E, Humborg C, Kortelainen P, Durr H, Meybeck M, Ciais P,

720   Guth P. 2013. Global carbon dioxide emissions from inland waters. *Nature* **503**: 355-

721   359. DOI: 10.1038/nature12760.

722   Raymond PA, Oh N-H, Turner RE, Broussard W. 2008. Anthropogenically enhanced fluxes

723   of water and carbon from the Mississippi River. *Nature* **451**: 449-452. DOI:

724   10.1038/nature06505.

725   Richey JE, Melack JM, Aufdenkampe AK, Ballester VM, Hess LL. 2002. Outgassing from

726   Amazonian rivers and wetlands as a large tropical source of atmospheric CO2.

727   *Nature* **416**: 617-620. DOI: 10.1038/416617a.

728   Rosa E, Gaillardet J, Hillaire-Marcel C, Hélie J-F, Richard L-F. 2012. Rock denudation rates

729   and organic carbon exports along a latitudinal gradient in the Hudson, James, and

730   Ungava bays watershed. *Canadian Journal of Earth Sciences* **49**: 742-757. DOI:

731   10.1139/e2012-021.

732   Schröder B. 1968. *Erläuterungen zur Geologischen Karte von Bayern 1:25000 - Blatt Nr.*

733   *6332 Erlangen Nord*. Bayerisches Geologisches Landesamt; 159.

734   Seitzinger SP, Mayorga E, Bouwman AF, Kroeze C, Beusen AHW, Billen G, Van Drecht G,

735   Dumont E, Fekete BM, Garnier J, Harrison JA. 2010. Global river nutrient export: A

736   scenario analysis of past and future trends. *Global Biogeochemical Cycles* **24**:

737   GB0A08. DOI: 10.1029/2009GB003587.

738   Semhi K, Amiotte Suchet P, Clauer N, Probst JL 2000. Impact of nitrogen fertilizers on the

739   natural weathering- erosion processes and fuvial transport in the Garonne basin.

740   *Applied Geochemistry* **15**: 865-878. DOI: 10.1016/S0883-2927(99)00076-1.

741   Soulsby C, Tetzlaff D, van den Bedem N, Malcolm IA, Bacon PJ, Youngson AF. 2007.

742   Inferring groundwater influences on surface water in montane catchments from

743   hydrochemical surveys of springs and streamwaters. *Journal of Hydrology* **333**: 199-

744   213. DOI: 10.1016/j.jhydrol.2006.08.016.

745   Stögbauer A, Strauss H, Arndt J, Marek V, Einsiedl F, van Geldern R. 2008. Rivers of North-

746   Rhine Westphalia revisited: Tracing changes in river chemistry. *Applied*

747   *Geochemistry* **23**: 3290-3304. DOI: 10.1016/j.apgeochem.2008.06.030.

748   Struyf E, Smis A, Van Damme S, Meire P, Conley DJ. 2009. The Global Biogeochemical

749   Silicon Cycle. *Silicon* **1**: 207-213. DOI: 10.1007/s12633-010-9035-x.

750   Sun H, Alexander J, Gove B, Pezzi E, Chakowski N, Husch J. 2014. Mineralogical and

751   anthropogenic controls of stream water chemistry in salted watersheds. *Applied*

752   *Geochemistry* **48**: 141-154. DOI: 10.1016/j.apgeochem.2014.06.028.

753   Szramek K, McIntosh JC, Williams EL, Kanduc T, Ogrinc N, Walter LM. 2007. Relative

754   weathering intensity of calcite versus dolomite in carbonate-bearing temperate zone

755   watersheds: Carbonate geochemistry and fluxes from catchments within the St.

756   Lawrence and Danube river basins. *Geochemistry, Geophysics, Geosystems* **8**. DOI:

757   10.1029/2006GC001337.

758   Torres MA, Baronas JJ, Clark KE, Feakins SJ, West AJ. 2017. Mixing as a driver of temporal

759   variations in river hydrochemistry: 1. Insights from conservative tracers in the

760   Andes-Amazon transition. *Water Resources Research* **53**: 3102-3119. DOI:

761   10.1002/2016WR019733.

762   van Geldern R, Schulte P, Mader M, Baier A, Barth JAC. 2015. Spatial and temporal

763   variations of pCO$_2$, dissolved inorganic carbon and stable isotopes along a temperate

764   karstic watercourse. *Hydrological Processes* **29**: 3423-3440. DOI:

765   10.1002/hyp.10457.

766   Verma MP, Portugal E, Gangloff S, Armienta MA, Chandrasekharam D, Sanchez M,

767   Renderos RE, Juanco M, van Geldern R. 2015. Determination of carbonic species

768   concentration in natural waters - Results from a worldwide proficiency test.

769   *Geostandards and Geoanalytical Research* **39**: 233-255. DOI: 10.1111/j.1751-

770   908X.2014.00306.x.

771   Viers J, Dupré B, Gaillardet J. 2009. Chemical composition of suspended sediments in World

772   Rivers: New insights from a new database. *Science of the Total Environment* **407**:

773   853-868. DOI: 10.1016/j.scitotenv.2008.09.053.

774   Voss BM, Peucker-Ehrenbrink B, Eglinton TI, Fiske G, Wang ZA, Hoering KA, Montluçon

775   DB, LeCroy C, Pal S, Marsh S, Gillies SL, Janmaat A, Bennett M, Downey B,

776   Fanslau J, Fraser H, Macklam-Harron G, Martinec M, Wiebe B. 2014. Tracing river

777   chemistry in space and time: Dissolved inorganic constituents of the Fraser River,

778   Canada. *Geochimica et Cosmochimica Acta* **124**: 283-308. DOI:

779   10.1016/j.gca.2013.09.006.

780   White WB. 1988. *Geomorphology and hydrology of karst terrains*. Oxford University Press,

781   New York; 464.

782   Widory D, Petelet-Giraud E, Brenot A, Bronders J, Tirez K, Boeckx P. 2013. Improving the

783   management of nitrate pollution in water by the use of isotope monitoring: the δ^{15}N,

784   δ^{18}O and δ^{11}B triptych. *Isotopes in Environmental and Health Studies* **49**: 29-47.

785   DOI: 10.1080/10256016.2012.666540.

786   Williams P, Fong YT. 2010. World Map of Carbonate Rock Outcrops v3.0. Accessible at

787   http://web.env.auckland.ac.nz/our_research/karst/.

788   Williams PW, Ford DC. 2006. Global distribution of carbonate rocks. *Zeitschrift für*

789   *Geomorphologie Supplement* **147**: 1-2.

790   Winter T, Harvey J, Franke O, Alley W. 1998. *Groundwater and surface water - A single*

791   *resource*. US Geological Survey Circular 1139; 79.

792   Wippern J. 1955. *Erläuterungen zur Geologischen Karte von Bayern 1: 25000 - Blatt Nr.*

793   *6134 Waischenfeld*. Bayerisches Geologisches Landesamt; 47.

794   Wollast R, Mackenzie FT. 1983. The global cycle of silica. In: *Silicon geochemistry and*

795   *biochemistry*, Aston SR (ed.) Academic Press, San Diengo; pp: 39-76.

796   Yang C, Telmer K, Veizer J. 1996. Chemical dynamics of the "St. Lawrence" riverine

797   system: δD_{H2O}, $\delta^{18}O_{H2O}$, $\delta^{13}C_{DIC}$, $\delta^{34}S_{sulfate}$, and dissolved $^{87}Sr/^{86}Sr$. *Geochimica et*

798   *Cosmochimica Acta* **60**: 851-866. DOI: 10.1016/0016-7037(95)00445-9.

799   Zavadlav S, Kanduč T, McIntosh J, Lojen S. 2013. Isotopic and Chemical Constraints on the

800   Biogeochemistry of Dissolved Inorganic Carbon and Chemical Weathering in the

801   Karst Watershed of Krka River (Slovenia). *Aquatic Geochemistry* **19**: 209-230. DOI:

802   10.1007/s10498-013-9188-5.

803   Zhang J, Zhang ZF, Liu SM, Wu Y, Xiong H, Chen HT. 1999. Human impacts on the large

804   world rivers: Would the Changjiang (Yangtze River) be an illustration? *Global*

805   *Biogeochemical Cycles* **13**: 1099-1105. DOI: 10.1029/1999GB900044.

806

807

808   **FIGURE CAPTIONS**

809   Figure 1. Location of the study area in Southern Germany, sampling points and lithology of

810   the Wiesent catchment. Sampling points are indicated for the Wiesent main river (numbers in

811   circles) and tributaries (numbers in square boxes). The total area of the Wiesent Catchment is

812    $1,040\ km^2$.

813

814   Figure 2. Schematic hydrogeologic cross section of the northern Franconian Alb (modified

815   after (modifed after Apel and Büttner, 1995). Lias, Dogger, and Malm are German regional

816   names of Jurassic series.

817

818   Figure 3. Land cover along the Wiesent River and tributaries. Data is based on the CORINE

819   Land Cover 2006 (CLC 2006) and the hydrographic reference set EU-Hydro of the European

820   Union Copernicus Land Monitoring Service (https://land.copernicus.eu).

821

822   Figure 4. Major ion chemistry, electric conductivity (EC), and temperature (T) along the

823   Wiesent River. Additional data (pH, O_2, environmental isotopes, discharge, precipitation) is

824   available from the Supplementary Material to this article and from van Geldern *et al.* (2015).

825

826   Figure 5. Piper diagram for the Wiesent River and sampled tributaries. Numbers in

827   parentheses refer to sampling locations. The tributaries Truppach (10) and Puettlach (12)

828   mainly drain claystone and sandstone dominated lithology.

829

830   Figure 6. (A) Ca^{2+} plus Mg^{2+} plotted against HCO_3^- concentrations (expressed in meq L^{-1}) of

831   the Wiesent River. The dashed line indicates the stoichiometric relation of carbonate

832   weathering. (B) Na$^+$ plus K$^+$ plotted against Cl$^-$ concentrations (expressed in meq L^{-1}). The

833   dashed line indicates the stoichiometric relationship for salt dissolution.

TABLES

Table 1. Long-term nitrate concentrations (1985 – 2015, arithmetic annual means) measured at the water quality monitoring station located at the lower Wiesent river course ("Reuth, KW Oberwasser", station ID 18423). Data available from the Bavarian Environmental Agency (LfU) at http://www.gkd.bayern.de (last accessed 20 January 2018).

calendar year	NO_3^- /mg L^{-1}	number of value per year
1985	18.2	24
1986	20.3	27
1987	19.0	27
1988	18.2	26
1989	18.9	27
1990	18.8	26
1991	19.3	26
1992	18.5	26
1993	20.2	26
1994	19.4	26
1995	20.6	26
1996	19.1	26
1997	19.9	27
1998	19.9	26
1999	20.4	26
2000	21.3	26
2001	19.8	26
2002	20.1	25
2003	19.5	26
2004	20.6	26
2005	20.9	26
2006	20.3	25
2007	20.7	26
2008	20.3	24
2009	19.6	26
2010	19.0	25
2011	19.9	25
2012	18.6	26
2013	17.7	26
2014	17.6	13
2015	18.2	13
average	(19.5 ± 1.0)	
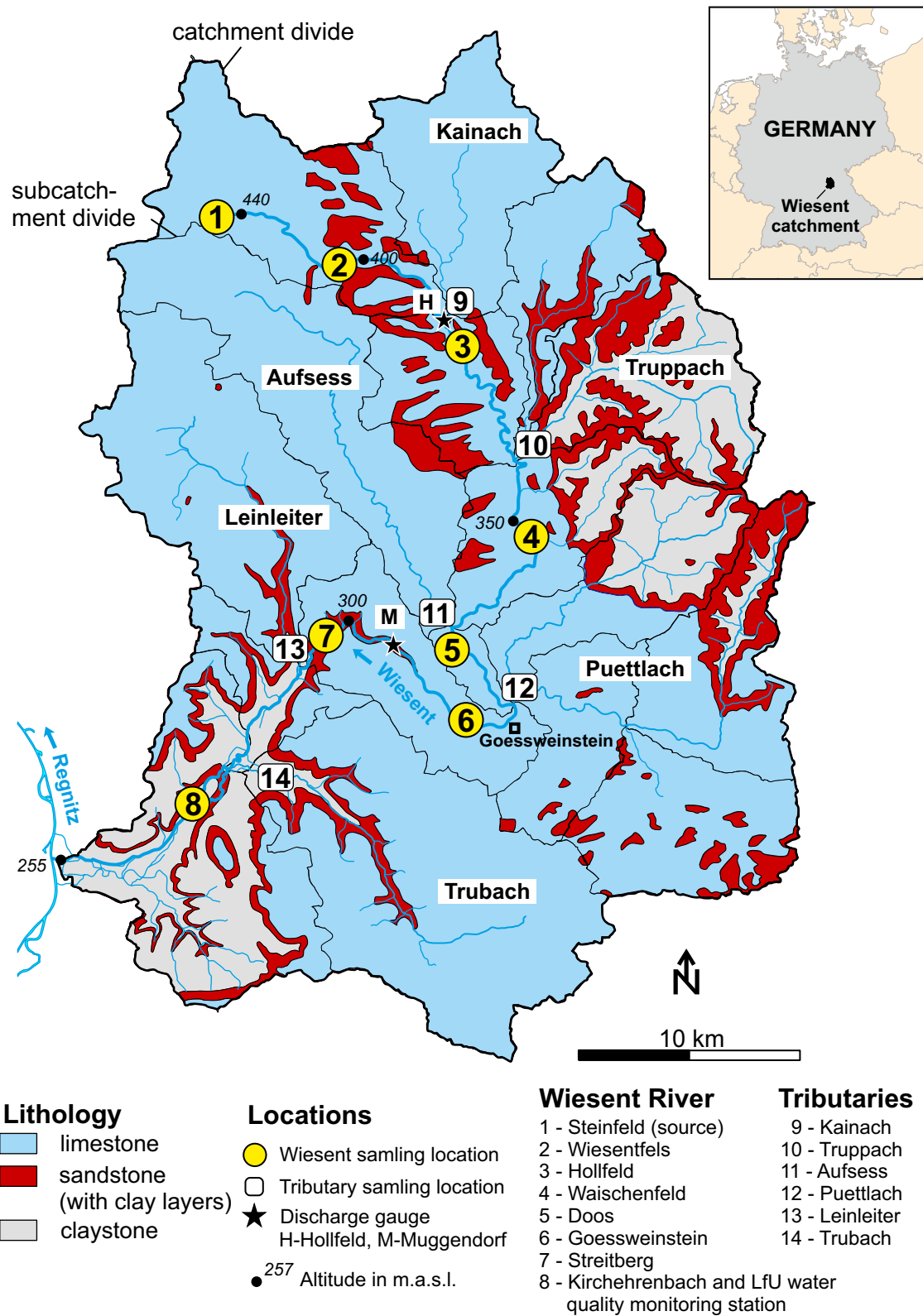
Figure 1. Location of the study area in Southern Germany, sampling points and lithology of the Wiesent catchment. Sampling points are indicated for the Wiesent main river (numbers in circles) and tributaries (numbers in square boxes). The total area of the Wiesent Catchment is 1,040 km2.
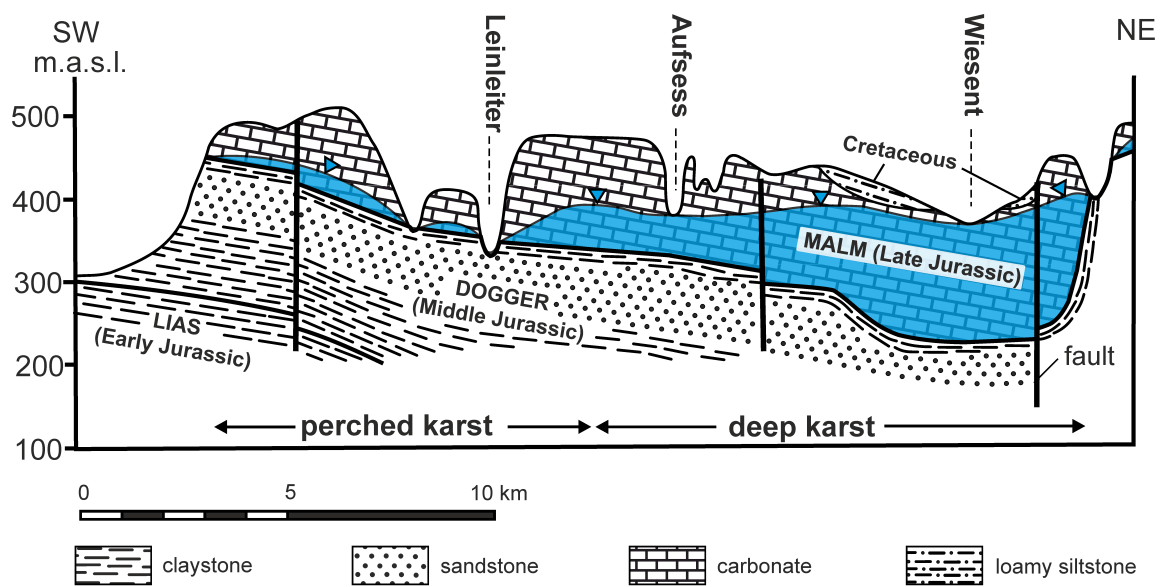
Figure 2. Schematic hydrogeologic cross section of the northern Franconian Alb (modified after (modifed after Apel and Büttner, 1995). Lias, Dogger, and Malm are German regional names of Jurassic series.
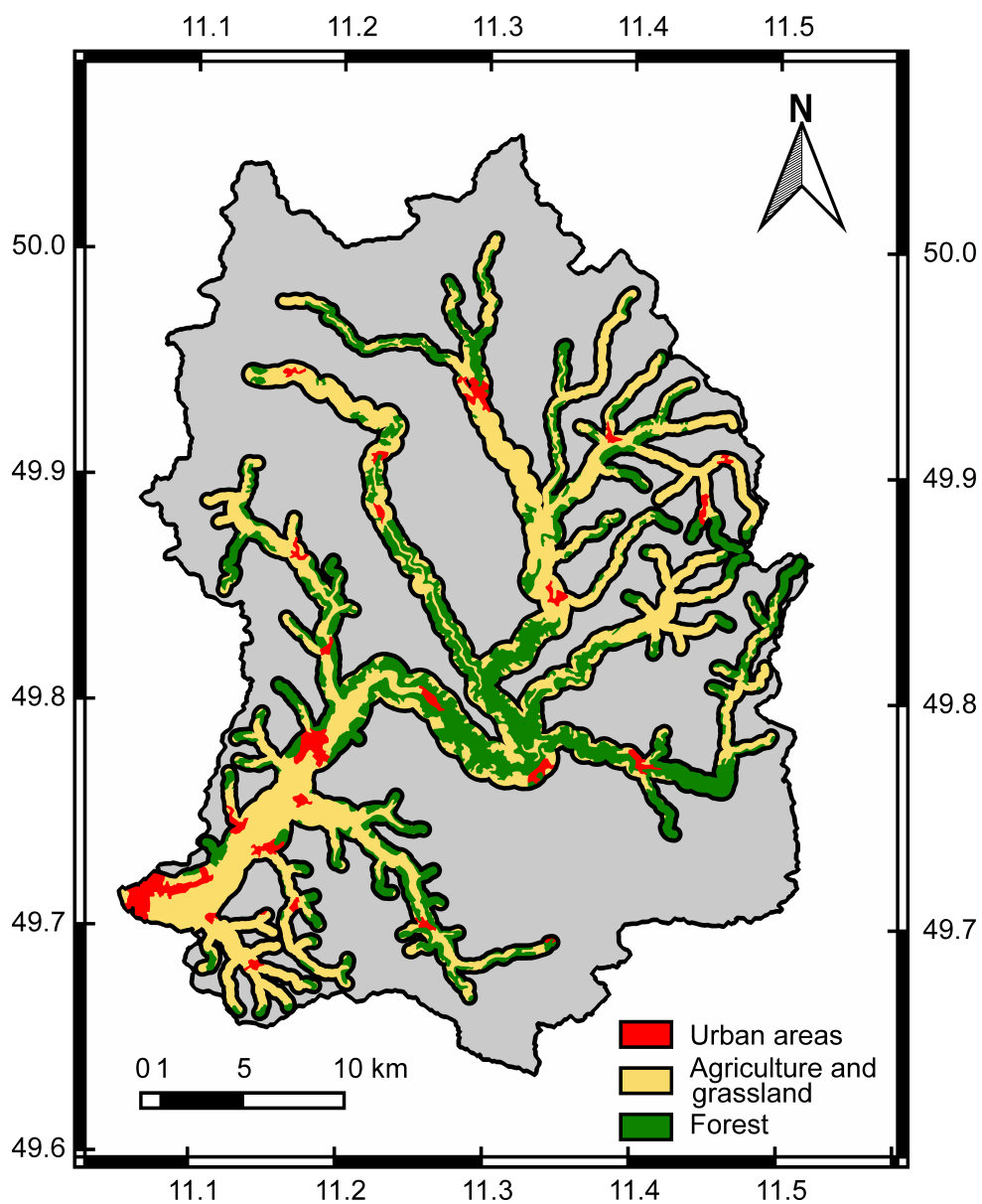
Figure 3. Land cover along the Wiesent River and tributaries. Data is based on the CORINE Land Cover 2006 (CLC 2006) and the hydrographic reference set EU-Hydro of the European Union Copernicus Land Monitoring Service (https://land.copernicus.eu).
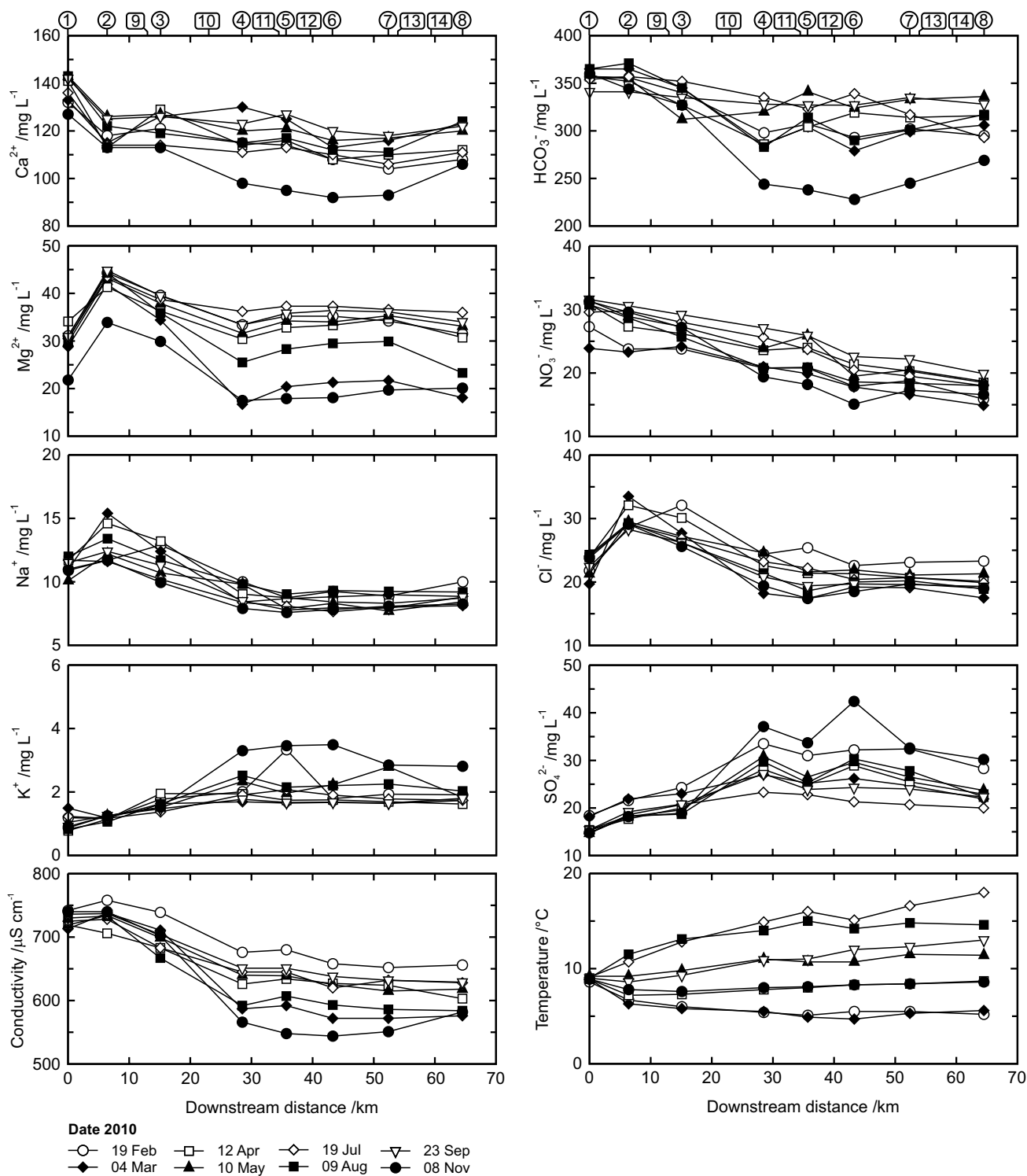
Figure 4. Major ion chemistry, electric conductivity (EC), and temperature (T) along the Wiesent River. Additional data (pH, O2, environmental isotopes, discharge, precipitation) is available from the Supplementary Material to this article and from van Geldern et al. (2015).
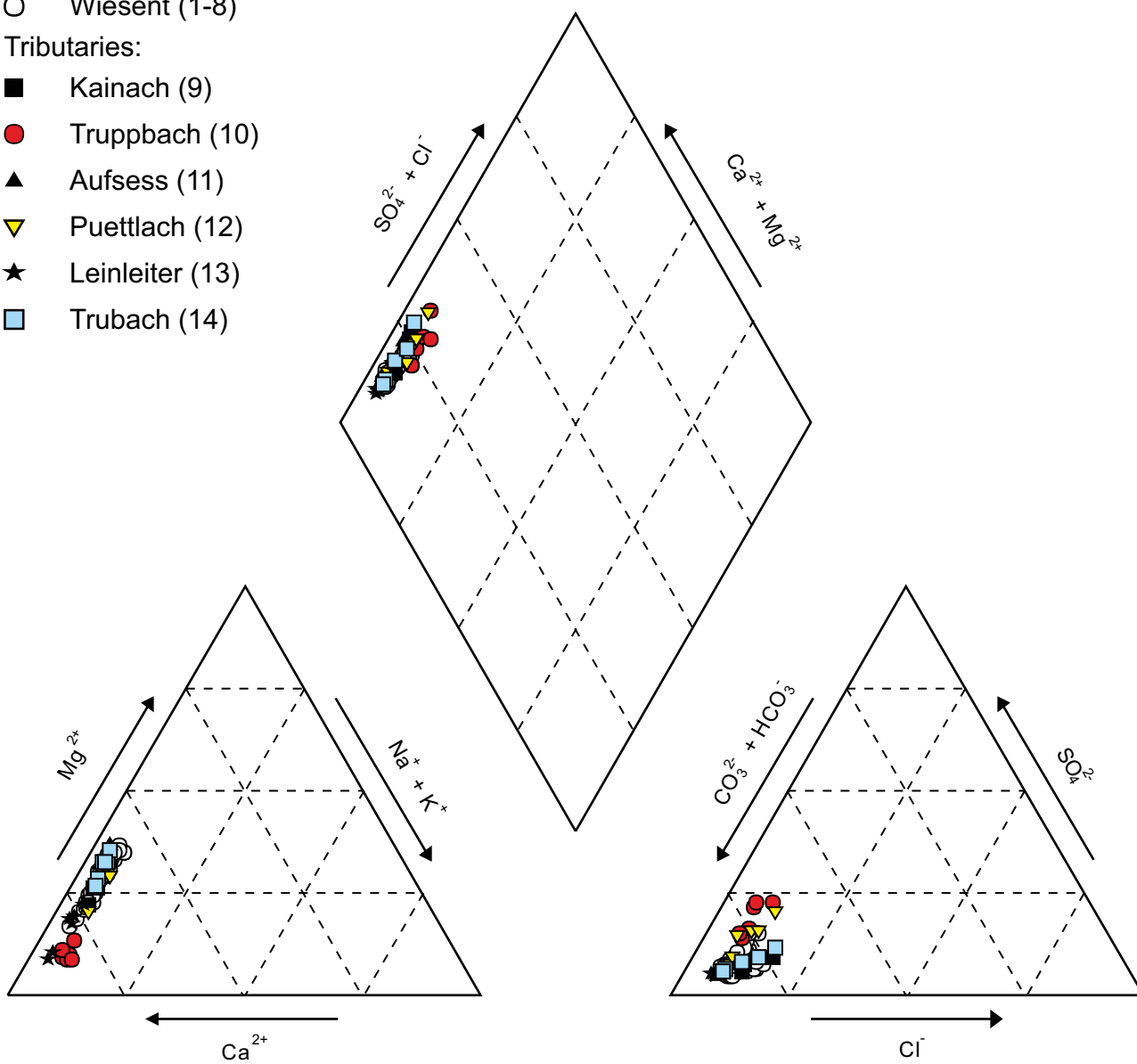
Figure 5. Piper diagram for the Wiesent River and sampled tributaries. Numbers in parentheses refer to sampling locations. The tributaries Truppach (10) and Puettlach (12) mainly drain claystone and sandstone dominated lithology.
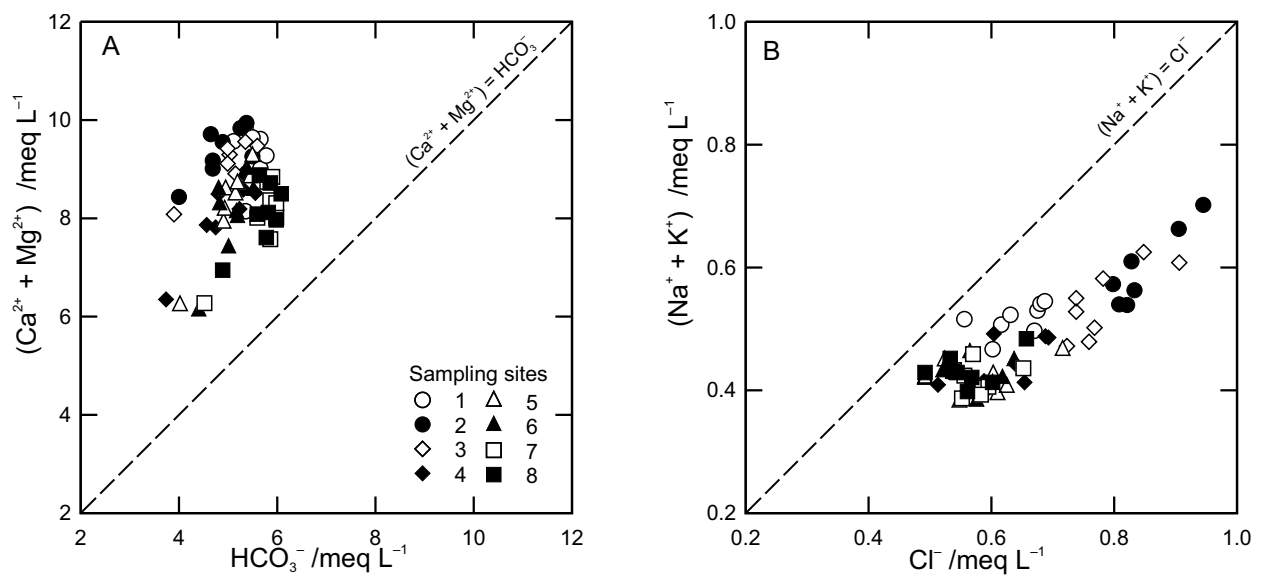
Figure 6. (A) Ca2+ plus Mg2+ plotted against HCO3- concentrations (expressed in meq L–1) of the Wiesent River. The dashed line indicates the stoichiometric relation of carbonate weathering. (B) Na+ plus K+ plotted against Cl- concentrations (expressed in meq L–1). The dashed line indicates the stoichiometric relationship for salt dissolution.